Soft Matter

View Online
Dynamic Article Links

Cite this: DOI: 10.1039/c0sm01312a

www.rsc.org/softmatter

PAPER

Rheology of globular proteins: apparent yield stress, high shear rate viscosity and interfacial viscoelasticity of bovine serum albumin solutions†

Vivek Sharma,[a] Aditya Jaishankar,[a] Ying-Chih Wang[b] and Gareth H. McKinley*[a]

Received 13th November 2010, Accepted 24th February 2011
DOI: 10.1039/c0sm01312a

Globular proteins influence the flow, microstructure, phase behavior and transport of biofluids and biomolecules in the mammalian body. These proteins are essential constituents of food, drugs and cosmetics, and their dynamics determine the physical properties and application of these multicomponent materials. In conventional rheological studies conducted using typical geometries on torsional rheometers, solutions of globular proteins are commonly reported to have a solid-like response at concentrations as low as 0.03% by weight. Typical explanations invoke the presence of long-range repulsions that are stronger than electrostatic interactions. In this study, we probe the bulk and the interfacial viscoelasticity of surfactant-free bovine serum albumin (BSA) solutions using a stress-controlled torsional rheometer, augmented by microfluidic rheometry and interfacial rheometric measurements. We demonstrate that the origin of this yield-like behavior, which is manifested as a highly shear-thinning bulk rheological response, lies in the formation of a film of adsorbed protein, formed spontaneously at the solution/gas interface. We provide direct interfacial rheometric measurements to study the concentration-dependent viscoelasticity of the adsorbed protein and we describe a simple, but quantitative, additive model useful for extracting the interfacial viscosity contribution from bulk viscosity measurements over a wide range of shear rates.

1. Introduction

Serum albumins are the most abundant among the constituent proteins in mammalian blood.[1] Serum albumins participate in various biological functions, including maintaining blood pH and osmotic pressure,[2] as well as transporting ligands, metabolites, lipophilic compounds, hormones and drugs, including anesthetics and anti-coagulants.[1,2] Since albumins transport all kinds of cargo, Peters refers to them as the "tramp steamers" of blood circulation.[1] The concentration of human serum albumin (HSA) in blood plasma is ~40 mg ml^{-1} (~0.6 mM). Bovine serum albumin (BSA) is quite similar to human serum albumin (HSA) (80% homology).[1] Interestingly, when BSA solutions are tested on a torsional rheometer, the solutions exhibit a yield-like behavior for a relatively wide range of concentrations (0.03–10 wt%),[3–5] with the apparent viscosity dropping by several orders of magnitude as the imposed shear rate is raised from 0.01 to 100 s^{-1}. Similar responses have been observed for other globular proteins.[6–9] It is argued that the presence of a yield stress is a consequence of strong long-range repulsive forces that are present even at concentrations as low as 0.03 wt% (or 0.3 mg ml^{-1}), and the concentration of added salts is reported to have little or no effect on the observed response.[5] Several recent studies invoke this apparent yield stress of solutions of bovine serum albumin and other proteins in the context of applications ranging from electrospinning[10] to synovial lubrication,[11] and in the discussion of glassy behavior exhibited by BSA solutions at high concentration.[12] Since the interactions of these proteins affect osmotic properties, functioning and flow of blood and play a critical role in various physiological processes, clinical medicine and pharmacology,[1] the origin of this solid-like response, especially at relatively low concentrations of the globular protein solutes, needs to be examined and evaluated carefully and rigorously.

In this study, we characterize the bulk rheological behavior of BSA solutions by imposing steady shearing deformations on a stress-controlled rotational rheometer using both cone-and-plate (CP) and double-gap (DG) Couette geometries. Since many proteins are known to adsorb preferentially at the solution/air interface that is ubiquitous in these geometries, we also use microfluidic rheometry to study the response of protein solutions in a device where no solution/air interface is present. Interestingly, we measure an apparent yield-like response for BSA solutions with the two torsional fixtures, but not in the microfluidic chip, implying that interfacial rheological effects may be important. It is well known that measurements of material properties such as surface tension on a static fluid interface do not provide a quantitative understanding of the dynamical response of the

[a]*Hatsopoulos Microfluids Laboratory, Department of Mechanical Engineering, Massachusetts Institute of Technology, Cambridge, MA, 02139-4307, USA. E-mail: gareth@mit.edu*
[b]*Rheosense Inc, San Ramon, CA, USA*
† Electronic supplementary information (ESI) available. See DOI: 10.1039/c0sm01312a

interface.[13–15] Therefore, we also probed the rate-dependent interfacial viscosity and strain-dependent interfacial viscoelasticity of the BSA solutions using a novel double wall ring (DWR) geometry.[16] This detailed study of interfacial rheology is necessary to distinguish the contribution from globular proteins in solution from that of proteins adsorbed at the interface.

In general, the viscoelasticity of a protein or colloidal solution is a manifestation of both the increased resistance to flow that originates from the friction experienced by the dispersed moieties, and from the strength of interactions that must be overcome to cause any deformation from an undisturbed state. The interparticle interactions and microstructure deduced from the response to an imposed stress must also influence the hydrodynamic and thermodynamic properties measured in diffusion, osmotic pressure and scattering experiments;[17,18] therefore we also compare and contrast the range of interaction potentials obtained with different techniques (see Section 3.4). Finally, we derive a simple but quantitative model to show how typical bulk viscosity measurements made on a torsional rheometer in the presence of a free surface can be systematically interpreted in terms of a rate-independent bulk contribution (measured with microfluidic rheometry at high shear rates) and a non-linear, rate-dependent interfacial contribution. We hope that our measurements, theoretical insights and discussion will provide the context and methodology for deconvolving the complex rheological behavior of other biofluids where such interfacial effects play a role.

The characterization and understanding of interfacial rheological properties of proteins, surfactants, macromolecules and particles are important for many applications including food,[19–21] foam and emulsion stability,[22] medicine and biology,[15,23,24] oil recovery, high speed coating,[14] *etc.* Many researchers have studied and described the orientational and conformational changes of proteins in interfacial environments and these changes markedly influence the viscoelastic nature of the interface.[25–28] Typical biofluids encountered in nature and in industry are multicomponent mixtures and the structure and the rheology of the complex mixed interface depend upon the concentrations and interactions of the different surface-active components.[15,23,29–31] In this study, we focus specifically on the rheology of surfactant-free protein solutions to understand, in a quantitative way, why dilute solutions of globular proteins (such as bovine serum albumin solutions) display a yield-like behavior in bulk viscosity measurements on a torsional rheometer. Similar apparent solid-like behavior has been observed in bulk rheology measurements on physiological fluids in biomedical applications (*e.g.* whole saliva),[32,33] pharmaceuticals (*e.g.* monoclonal antibody solutions, see discussion later)[34–36] and, most commonly, in the food and consumer product industries (*e.g.* acacia gum solutions),[37] among others. The non-Newtonian bulk rheological response as measured with a cone-and-plate geometry was attributed to the formation of an interfacial viscoelastic film by Waterman *et al.* for saliva solutions[32] and similar qualitative arguments are put forward by Sanchez *et al.* for acacia gum solutions.[37] By making distinct independent measurements of the interfacial viscosity and the interface-free bulk response of the protein solutions, in the present work we are able to isolate and quantify the effect of the interfacial viscoelastic film. Using a simple additive model, we show how the presence of a viscoelastic solid-like film will systematically corrupt the measured bulk viscosity on conventional torsional rheometers for most biofluids and solutions containing surface-active groups. Further, we show how the effective contribution of the interfacial film to the apparent measured viscosity changes with the choice of geometry on a torsional rheometer, and we provide an analytical method for estimating both the interfacial viscosity and true zero shear viscosity from bulk viscosity measurements.

2. Background

2.1 Interfacial rheometry with double wall ring (DWR)

Interfacial rheometry probes the microstructure and dynamics of thin layers or films or skins formed on interfaces of surfactant, protein or macromolecular solutions, by measuring the response to either a compressional/dilational deformation or a shear deformation.[13–15,20,38] At equilibrium, the interface exhibits a state of tension, which is quantified in terms of a force per unit length or surface tension, σ (units: N m^{-1} or Pa m). For a given solution, the interfacial tension varies with concentration, temperature and bulk-phase pressure, and any gradient in these parameters creates a surface tension gradient that can drive so-called Marangoni flows at the interface as well as in bulk.[13,14] These flows encounter additional dampening by viscous stresses generated at the interface, which can be parameterized by an interfacial viscosity, η_s (units: Pa s m), characterizing the surface drag.[14] A constitutive relation between the interfacial shear stress, $\boldsymbol{\tau}_s$ (Pa m), and interfacial shear rate $\dot{\gamma}$ (s^{-1}), was first proposed by Boussinesq, and the Boussinesq–Scriven surface stress tensor for Newtonian-like interfaces is given by[14,38,39]

$$\boldsymbol{\tau}_s = [(\kappa_s - \eta_s)\nabla_s\vec{v}_s]\boldsymbol{P}_{st} + 2\eta_s\boldsymbol{D}_s \quad (1)$$

where κ_s is the interfacial dilational viscosity, $\boldsymbol{D}_s$ is the rate of deformation tensor, $\nabla_s\vec{v}_s$ is the divergence of the interfacial velocity, and $\boldsymbol{P}_{st}$ is a projection tensor that transforms the vector contributions into the component tangential to the interface. In the more general non-Newtonian case that is expected when high molecular weight solutes such as proteins are adsorbed on the surface, the relation between interfacial stress and interfacial deformation is nonlinear[14,15] and the interfacial viscosity depends upon the two principal invariants of the surface deformation tensor. In addition to an interfacial viscosity, η_s, viscoelastic interfaces also exhibit an interfacial viscoelasticity, G_s^* (units Pa m). By analogy with bulk oscillatory measurements, the linear response of the interface to an oscillatory shear strain, $\gamma(\omega) = \gamma_0 \sin(\omega t)$ can be quantified at small amplitudes in terms of a frequency-dependent dynamic surface elasticity, $G_s^*(\omega) = G_s'(\omega) + iG_s''(\omega)$ where the real and imaginary part correspond to the interfacial storage and loss modulus respectively. The different methods used traditionally for measuring interfacial rheology for food proteins, surfactant–protein mixtures and biofluids used in medical diagnostics are detailed elsewhere.[14,15,38,40] Here we limit the discussion to the interplay between the interfacial and bulk rheology of surfactant-free globular proteins.

As a result of the boundary conditions at the interface, in typical rheological measurements, the deformation imposed on the interface becomes coupled with a corresponding deformation or flow in the bulk phases.[14,15] The challenge is to deconvolute the

bulk and the interfacial contributions. The contribution of surface drag relative to bulk drag for a steady shear flow is described by the Boussinesq number, Bo_s, defined as

$$Bo_s = \frac{(\eta_s V/L_s)P_s}{(\eta V/L_B)A_B} = \frac{\eta_s}{\eta l_s} \quad (2)$$

where V is a characteristic velocity (units: m s^{-1}) L_s and L_B are the characteristic length scales for shear flow in the interface and bulk sub-phase respectively, P_s is the contact perimeter between the interface and the probe (units: m) and A_B is the contact area between the geometry and the sub-phase (units: m^2). The effects of interfacial viscosity dominate only for $Bo_s \gg 1$ and can be maximized by choosing a geometry that maximizes the wetted perimeter for a given contact area, or equivalently by minimizing the characteristic length scale, $l_s \approx A_B/P_s$.[14] In the DWR set-up,[16] this ratio is $l_s \approx A_B/P_s = 0.7$ mm, which results in a reasonably high Boussinesq number, even for moderate values of η_s/η. Specifically, the characteristic length scale is 48 times smaller than the corresponding value for a bi-cone geometry with a radius of 34 mm,[38] thus allowing higher values of Bo_s and improved instrumental sensitivity to interfacial effects. The corresponding expressions for the Boussinesq number in the cone-and-plate (CP) geometry, $Bo_s^{CP} = 2\eta_s/\eta R$ and double-gap (DG) geometry, $Bo_s^{DG} = \eta_s/\eta L$ indicate that interfacial contributions will always be much smaller than those for the DWR fixture, because the cylinder length, L, in DG and cone radius, R, in CP are at least an order of magnitude greater than l_s for the DWR fixture. However, whether interfacial effects can be safely neglected entirely in these geometries depends intimately on the measured values of η_s/η.

The choice of the DWR geometry and the torque sensitivity of the torsional rheometer dictate the minimum measurable interfacial viscosity. In the set-up used in these experiments, with the minimum torque 0.02 μNm, an interfacial viscosity $\eta_s > 5 \times 10^{-6}$ Pa s m, can be measured. Lower values of interfacial viscosity can be measured by using a magnetic needle rheometer[41] or by using 2D microrheology (accessing values as low as 10^{-10} Pa s m). Whereas the magnetic needle rheometer uses a rod of several hundred microns in length, 2D microrheology relies on video-tracking of the thermal motion (2D Brownian motion) of passive tracer particles that are only few microns in diameter. The magnetic rod rheometer requires a range of rod sizes to achieve the dynamic range easily achieved using the DWR ring. Two-dimensional microrheology works best for viscous and weakly viscoelastic interfaces in which the mean square displacement (MSD) of the particles is linear in time, and the diffusion coefficient can then be related to the viscosity of the medium using the Stokes–Einstein equation.[42] For heterogeneous interfaces, more accurate results require two-particle tracking,[43,44] and for complex interfaces, where the mean square displacement has a sub-linear dependence on time, a generalized version of the Stokes–Einstein (GSE) equation must be used.[42,45] In such cases the interpretation of the mean square displacement data requires use of hydrodynamic models and additional assumptions (as summarized by Ortega *et al.*[42]), and connections with bulk measurements are relatively difficult to make.[42] For the stiff viscoelastic interfaces described in this study, the use of the DWR geometry provides an easy and accurate measurement technique over a wide dynamic range that is not easily achieved with 2D microrheology.

2. Materials and methods

2.1 Materials

Bovine serum albumin (BSA) solutions were prepared in Phosphate Buffered Saline (0.01 M PBS, pH = 7.4; Sigma-Aldrich). The solutions were refrigerated and were allowed to warm up to room temperature before experiments were carried out. The physico-chemical properties of BSA including structure, conformational changes under pH or temperature are well-documented,[1] and for the experimental conditions used here, the protein is in its globular form and is not denatured.

2.2 Method

In the DWR set-up, the sample is placed in the trough, and a circular ring with square cross-section is positioned at the interface. The DWR fixture (TA Instruments) is attached to a stress controlled rheometer (AR-G2, TA Instruments). The choice of a controlled stress rheometer is natural when studying phenomena such as elastoplastic deformation and yielding of complex fluids. The sensitivity of the instrument to interfacial contributions, control experiments with the DWR test fixture, as well as simulation of flows induced at the interface and in the bulk sub-phase are described in detail by Vandebril *et al.*[16] The specific geometrical parameters relevant to our set-up are the same as described in Vandebril *et al.*[16] Although in the present study we focused exclusively on the solution/air interface, a second (less dense) upper liquid can also be used. We note that because of the high surface concentration of the protein (and hence high interfacial viscosity), the Boussinesq number is high in all the DWR data reported in the paper. The non-linearity induced by the sub-phase flow can be neglected. We further checked for the possible effect of non-linearity using the MATLAB script from Vandebril *et al.*[16] (kindly provided by Jan Vermant), and confirmed that no correction was needed for these measurements on BSA solutions (see ESI† for details). The fluid used in the interfacial measurements was carefully drawn from the stock solution, without including the fluid from the liquid–air interface where pre-adsorbed protein is present. The sample was loaded into the trough and peak-hold experiments described in the next section were initiated immediately.

The bulk rheological response of BSA solutions was measured at 25 °C using a cone-and-plate (CP) geometry (2° cone, 40 mm) or a double-gap concentric cylinder fixture (DG) on the AR-G2. In addition, a microfluidic slit rheometer referred to as VROC (Viscometer-Rheometer-on-Chip, Rheosense Inc, CA) was employed to measure the steady shear viscosity of the solutions at high shear rates. The specific microfluidic device used in this study, mVROC Type A05 chipset, consists of a rectangular cross-section channel (w = 3.02 mm; d = 50 μm) made out of Pyrex mounted on a gold-coated silicon base containing three flush mounted pressure sensors.[46] The pressure drop, ΔP, required to drive the flow with rate, Q, is related to the wall shear stress, τ_w, by the expression $wd\Delta P = 2L(w + d)\tau_w$, whereas the nominal wall shear rate, $\dot{\gamma}_w$, associated with fully developed laminar flow of a Newtonian fluid is $\dot{\gamma}_w = 6Q/wd^2$. In a typical experiment, the flow rate, Q, is varied using a syringe pump and 2.5 ml Hamilton Gastight glass syringes (Reno, NV, USA). The VROC device outputs the pressure drop as a function of flow rate

and the data can then be used to determine the nominal or apparent viscosity $\eta(\dot{\gamma}) = \tau_w/\dot{\gamma}_w$. For a non-Newtonian, shear thinning fluid, the velocity profile in the channel will not be parabolic and the plot of ΔP *vs.* Q is nonlinear. In this case, the true wall shear rate can be computed using the Weissenberg–Rabinowitsch–Mooney (WRM) equation.[46] For a given channel, the range of wall shear rates, $\dot{\gamma}_w$, accessible is determined by the viscosity and shear thinning behavior of the fluid and the range of shear stresses, τ_w, is set by the choice of pressure sensors.

The maximum pressure, P_{max}, attainable in mVROC Type A05 used in the measurements conducted at MIT is $P_{max} = 10$ kPa. Since the measurable pressure range is nominally 1–100% of P_{max}, the minimum shear rate is $\dot{\gamma}_{w\ min} \approx 300\ s^{-1}$ for a viscosity of $\eta = 1$ mPa s. A parallel set of measurements were performed at Rheosense Inc, using mVROC Type A02 ($d = 20$ μm, as opposed to $d = 50$ μm for mVROC Type A05; same pressure range), this extended the measurable shear rate range to lower shear rates of $\dot{\gamma}_{w\ min} \approx 100\ s^{-1}$ for a viscosity of $\eta = 1$ mPa s. The temperature of fluid in the syringe as well as in the VROC channel and all interconnects was maintained at 25 °C using thermal jackets with a liquid circulation system.

3. Results and discussion

3.1 Bulk rheology and high shear rheometry

In stress sweep experiments, the steady shear viscosity, $\eta(\dot{\gamma})$ of bovine serum albumin (BSA) solutions, measured using the double-gap (DG) geometry on the controlled-stress rheometer, exhibits a highly shear thinning response, as seen in Fig. 1a. The data exhibit characteristics of a yield stress fluid[18] because $\eta(\dot{\gamma}) \approx \tau_Y/\dot{\gamma} \approx \dot{\gamma}^{-1}$. We also repeated the measurements using a cone-and-plate geometry (previous workers[3–5,10] have reported yield stress in BSA solutions primarily from CP geometry) and we obtained similar results.[3–10] We find that the viscosity measured with the DG is consistently lower than the CP measurements at all shear rates, as shown by the inset in Fig. 1a. Further, the relative viscosity of all the samples is nearly the same in the low shear rate regime, indicating that the characteristic concentration dependence expected for colloidal dispersions (discussed later) is not observed here.[17,18] We hypothesize that the high values of this nearly concentration-independent shear viscosity measured at low deformation rates must be related to the formation of an interfacial layer of adsorbed protein at the sample interface. The rheometric data suggest that the measured values of bulk viscosity obtained with either geometry have substantial contributions from a surface-adsorbed protein layer, and the relative contributions of interfacial effects depend upon the geometry. However to verify this hypothesis, we need to characterize the response of BSA solutions in a geometry that does not have any solution–gas interface.

For this purpose, we used the microfluidic capillary viscometer, VROC. The corresponding measurements indicate Newtonian-like response, as shown in Fig. 1a, with the rate-independent viscosity values increasing steadily with concentration, c, of BSA in solution. The VROC data agree quite well with the high shear rate viscosity measured in the DG, both approach a rate-independent value, $\eta_\infty(c)$. The viscosity values measured in VROC and DG are consistently lower than the viscosity

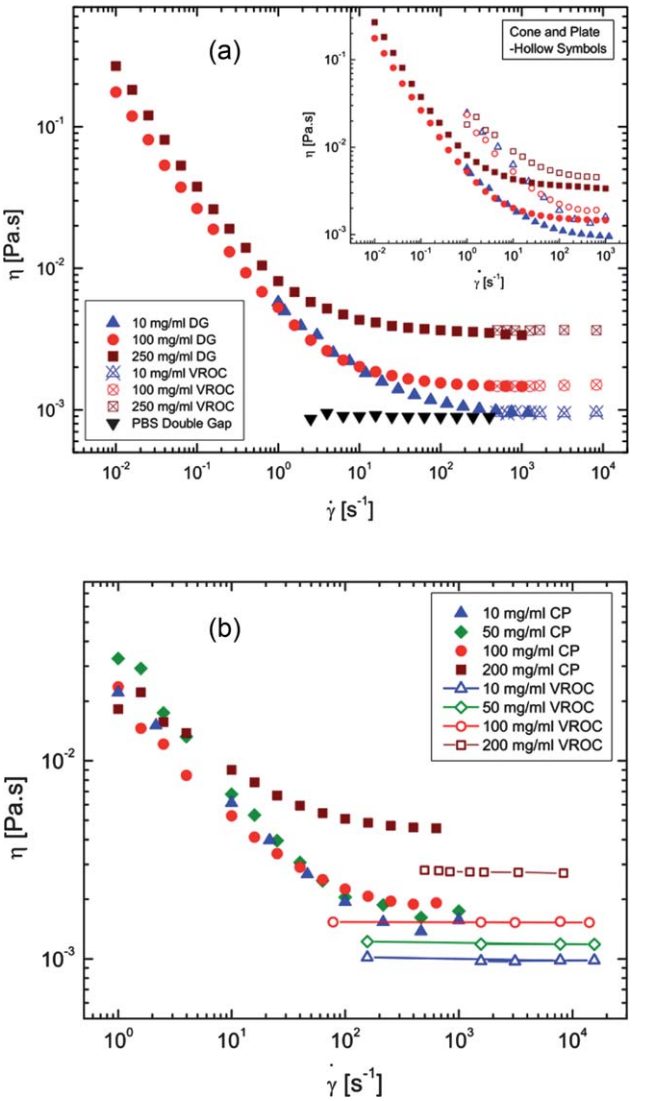

Fig. 1 Bulk steady shear viscosity of BSA solutions: (a) comparison of shear viscosity of BSA solutions measured using double gap geometry on a stress controlled rheometer (ARG2) (filled symbols), and a microfluidic rheometer (mVROC Type 05) (checked). The inset shows the bulk viscosity measured on ARG2 using double gap Couette (DG) geometry as contrasted with the 40 mm cone-and-plate geometry (CP) (hollow symbols). (b) Comparison of shear viscosity of BSA solutions measured using cone-and-plate on a stress controlled rheometer (ARG2) (filled symbols), and a microfluidic rheometer (mVROC Type 02, see text for details) (hollow symbols).

measured in CP geometry, especially at the lowest shear rates, $\dot{\gamma} \ll 10^3\ s^{-1}$. The difference between cone-and-plate and VROC measurements is even clearer when a different (more sensitive) microfluidic chip is used (experiments conducted at Rheosense Inc, San Ramon, CA using mVROC chip Type A02), which allows us to measure viscosity at lower shear rates than those possible with the chip Type A05 (used in MIT), as shown in Fig. 1b. The viscosity measured with different chips agrees quite well (see ESI†), though measurements using different geometries on a torsional rheometer show a geometry-dependent response as shown in Fig. 1a. It is clear that the protein-rich interface provides a much higher contribution to the overall response of

BSA solutions measured in rotational rheometers than the homogeneous solution examined in the interface-free flow generated in the microfluidic chip rheometer. The formation of a protein-rich interface and its deformation-rate-dependent viscosity and viscoelastic behavior are described in the next subsection.

3.2 Peak hold test and adsorption at the interface

After a fresh solution of BSA is placed in the DWR geometry, we can examine the change in interfacial viscosity by using a 'peak hold' test as shown in Fig. 2. The resistive torque exerted on the DWR fixture is measured as a function of time at a constant shear rate of $\dot{\gamma} = 1.5\ s^{-1}$. The resulting interfacial viscosity, η_s, increases steadily with time, and reaches a nearly constant value after 300 s. While the experimental protocol associated with filling the trough does not allow us to start the experiment immediately after the interface is created, the relative values of the rise in interfacial viscosity and the plateau viscosity are qualitative measures of the adsorption rate and concentration of the adsorbed protein, and the measured time scales are in good agreement with literature values.[47]

The driving force for adsorption of BSA at the surface can be understood by considering the thermodynamics of liquid interfaces.[13] The excess surface Gibbs free energy at an interface, G_I (units: J m^{-2}), can be related to the solute concentration by the Gibbs equation, $G_I = \sigma + \sum_i \mu_i \Gamma_i$, where μ_i is the chemical potential. The superficial density Γ_i is the two-dimensional concentration of surfactants in the interfacial region. Thus it follows from the Gibbs equation that if the surface tension of a liquid is lowered by the addition of a solute, the solute will be preferentially adsorbed at the interface. Like surfactants, BSA adsorbs at the liquid/air interface; the kinetics of adsorption, and the stability of the adsorbed film have been studied by a host of different techniques, including neutron reflectivity and spectroscopy,[48] ellipsometry and radiolabel technique,[49] fluorescence, surface tensiometry, microrheology,[47] surface pressure, as well as interfacial shear and dilational rheology.[20,50–52] It is well known that a saturated monolayer coverage develops as a result of nearly irreversible adsorption[49,53] and the kinetics of adsorption is diffusive only for low concentration of BSA (implying that the adsorbed amount increases with $t^{0.5}$).[49] For the relatively high bulk concentrations used in our experiments, a surface coverage of $\Gamma_i = 2$–3 mg m^{-2} of BSA is reported in the literature,[48,49] and this value of Γ_i is close to the maximum fractional coverage, Γ_{max}, expected for a configuration when ellipsoidal globular proteins lie sideways or with their long axis parallel to the interface.[48,49] Hence the interfacial viscosities measured in peak-hold experiments with the DWR geometry approach nearly identical, concentration-independent plateau values as shown in Fig. 2. The irreversible nature of the adsorption is demonstrated by the essentially unchanged value of the interfacial viscosity measured in each case when the shearing deformation is restarted after cessation for two minutes. While it is clear that protein adsorption leads to a significant interfacial viscosity contribution, the shear rate dependence of this adsorbed layer also needs to be studied, and is described in the next subsection.

3.3 Interfacial viscosity and viscoelasticity

The resistive torque exerted by the interface does not increase linearly as the rotational rate of the DWR is increased, leading to a marked shear thinning behavior in the measured value of interfacial viscosity as shown in Fig. 3. The data exhibit characteristics of a yield stress fluid as $\eta_s(\dot{\gamma}) \approx \tau_{sY}/\dot{\gamma} \sim \dot{\gamma}^{-1}$. This is strongly reminiscent of the bulk shear-thinning behavior reported in Fig. 1. In addition, there is no hysteresis seen in the

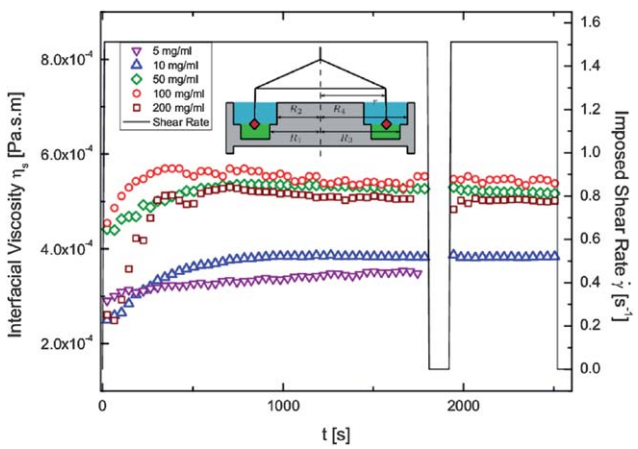

Fig. 2 Peak hold test characterizing the evolution of the interfacial viscosity for BSA samples tested using the DWR geometry, at a shear rate of 1.5 s^{-1} for 1800 s. After holding the sample at rest for 120 s, the viscosity measurement is repeated at the same shear rate. Schematic of double wall ring (DWR) fixture for interfacial rheometry (after ref. 25) is included. The ring has a square cross-section, with a width of 1 mm and is made out of platinum/iridium. The ring rests at the two-fluid interface, and in our case, the top fluid (blue) is air.

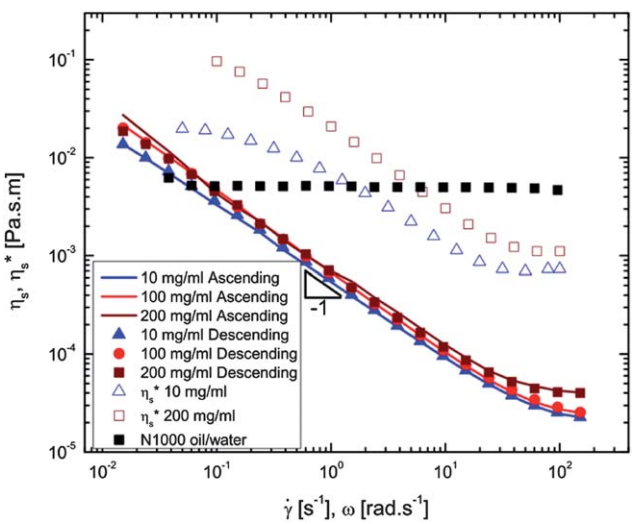

Fig. 3 Interfacial viscosity of BSA solution measured using ascending (symbols) and descending (lines) shear rate sweeps using the DWR geometry. The complex interfacial viscosity data (hollow symbols) measured in oscillatory shear with DWR show that the empirical Cox–Merz rule is not followed. A shear rate independent, Newtonian response is shown by a thin layer of calibration oil (N1000) on DI water (black squares).

measurement of η_s; values measured in ascending and descending shear-rate sweeps coincide in every case.

We estimate the diffusion timescale, t_D, for BSA to diffuse a distance equal to its size, a_{eff}, to be $t_D \approx a^2_{eff}/D \approx 0.2$ ms where $a_{eff} = 3.5$ nm, and D is determined using the Stokes–Einstein equation $D = kT/6\pi\eta_0 a_{eff}$ (where kT is the thermal energy and η_0 is the solvent viscosity). The estimated value (agrees with the measured value[54]) tells us that once the layer is established, in the absence of any other gradients, the superficial concentration of the macromolecules does not change due to diffusive transfer.[49] Additionally this explains why no hysteresis is observed in Fig. 3, because the interfacial layer reforms almost instantaneously after cessation of steady shear. To confirm whether this shear-thinning response is indeed from a non-Newtonian interfacial viscosity, we carried out calibration checks by mimicking the method of Vandebril *et al.*[16] Measurement with a film of viscous calibration oil (Cannon N1000) $\eta = 2.008$ Pa s with thickness, $\delta = 5.8$ mm formed over DI water is shown by black squares in Fig. 3. The measured Newtonian-like interfacial viscosity, $\eta_s = 0.59 \times 10^{-2}$ Pa s m, is greater than the simple estimate obtained by $\eta l_s = 0.14 \times 10^{-2}$ Pa s m (additional dissipation occurs in both oil and water phases).

To demonstrate the viscoelastic character of the interface, we compare the interfacial shear viscosity, η_s (filled symbols in Fig. 3), from steady shear experiments with the corresponding values of interfacial complex viscosity, η_s^*, obtained from small amplitude oscillatory shear measurements (hollow symbols). We find that the empirical Cox–Merz rule[18] stating $|\eta^*(\omega)| \cong \eta(\dot{\gamma})|_{\dot{\gamma}=\omega}$ is not obeyed. The lower values of $\eta_s(\dot{\gamma})$ imply that the interfacial microstructure of the adsorbed BSA film is disrupted by the larger shear deformations imposed during steady shear measurements. The strain-dependent values of interfacial storage and loss modulus measured in strain sweep experiments performed at a constant imposed frequency, $\omega = 1$ rad s^{-1} for various concentrations can be used to construct a viscoelastic master curve for this BSA interface as shown in Fig. 4. Here $a(c)$ and $b(c)$ are the shift factors required to overlay moduli data on the reference values measured at $c = 50$ mg ml^{-1}. For small strains and for the chosen frequency, the storage modulus is greater than the loss modulus, or $G_s'(\omega = 1$ rad s$^{-1}) > G_s''(\omega = 1$ rad s$^{-1})$, implying that the interface is rigid or solid-like. Increasing the concentration of BSA in solution is accompanied by increases in both the moduli. The measured interfacial elasticity falls rapidly beyond a yield strain, $\gamma_Y \approx 0.01$, and therefore the nominal interfacial tension required to break the interfacial structure (or cause the yielding of interfacial layer) is of the order of $\tau_{sY} = G_s'\gamma_Y = 2.3 \times 10^{-4}$ Pa m. It is worth noting that this value is close to the interfacial shear stress measured in steady shear, $\tau_{sY} = \eta_s\dot{\gamma} \approx 10^{-4}$ Pa m at the lowest imposed shear rates (10^{-2} s^{-1}) presented in Fig. 3.

The viscoelastic characteristics of the interface are further demonstrated by the frequency sweep measurements shown in Fig. 5. The elastic and viscous contributions to the interfacial shear modulus are shown by filled and hollow symbols respectively. At low frequencies, the interface response is dominated by viscous effects and $G_s'(\omega) < G_s''(\omega)$. The crossover frequency, ω^*, decreases, and the corresponding modulus values increase, with increasing concentration. The oscillatory shear measurements show that the interfacial microstructure becomes more gel-like

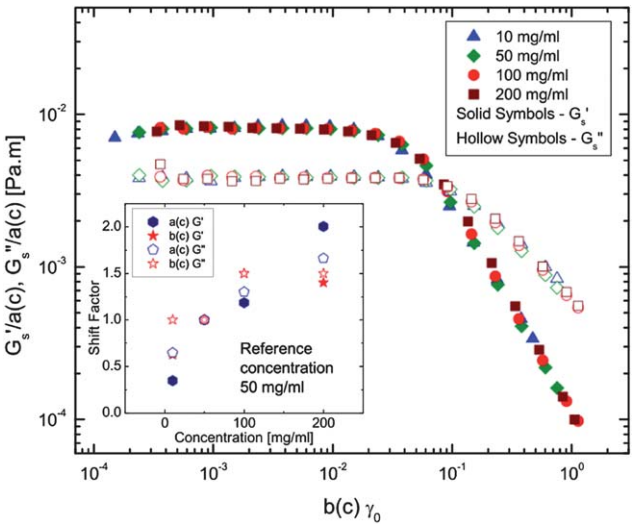

Fig. 4 Master-curve showing the reduced interfacial storage and loss modulus of BSA solutions measured as a function of reduced oscillatory strain amplitude at a fixed frequency using the DWR fixture on the ARG2. Shift factors construct the master curve as shown in the inset. All curves are overlaid on 50 mg ml^{-1} data.

with an increasing bulk concentration of the protein. It is well known[27,48] that the adsorption-induced conformation changes and subsequent protein aggregation at the liquid/air interface produce a viscoelastic film at the interface. The size and microstructure of protein aggregates as well as the presence of a secondary layer underneath the primary interfacial layer are reported to depend upon the concentration of protein in the bulk.[48] The lower crossover frequency observed at higher bulk concentrations corresponds to a longer relaxation time, implying that the interface has larger aggregates or more compactly packed protein in this case. By contrast, the interfacial shear viscosity data shown in Fig. 1 are measured at large imposed

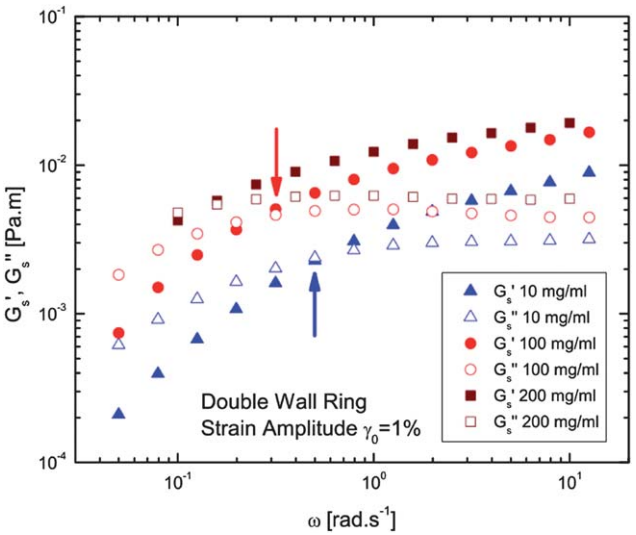

Fig. 5 Interfacial storage and loss modulus of BSA solutions measured as a function of oscillatory frequency for different values of BSA concentration (using DWR fixture). The arrows show the crossover frequency for the 10 mg ml^{-1} and 100 mg ml^{-1} concentrations respectively.

stresses, $\tau_s > \tau_{sY}$, that result in yielding and plastic flow. This yielding results in a nearly concentration-independent shear-thinning region, as seen in Fig. 1. The measurements at higher frequencies, *i.e.* for $\omega > 10$ rad s^{-1}, show significant inertial effects, where the raw phase angle approaches 180 degrees. The raw phase angle for the data shown in Fig. 5 is always less than 90 degrees, implying inertial contributions are properly accounted for. The importance of the inertial contribution can be evaluated using an appropriate Reynolds number, $Re = \rho\omega d^2/\eta$, for the present geometry where $d = 1$ mm is the characteristic dimension of the DWR geometry. For the BSA solutions, we find $Re > 1$ for $\omega > 1$ rad s^{-1}. The inertial contributions to the measured torque become prominent at high frequencies as was demonstrated and discussed by Reynaert *et al.*[41] for the magnetic rod rheometer and by Vandebril *et al.*[16] for the DWR geometry.

3.4 Intrinsic viscosity, charged suspensions and interaction potentials

The zero shear rate viscosity for colloidal suspensions is known to increase with concentration as described by the Krieger–Dougherty equation:[17,18]

$$\frac{\eta(\phi)}{\eta_0} = \left(1 - \frac{\phi}{\phi_m}\right)^{-[\eta]_s\phi_m} \quad (3)$$

where ϕ_m is the maximum packing fraction, $[\eta]_s = \lim_{\phi\to 0} -(\eta - \eta_0)/\phi\eta_0$ is the intrinsic viscosity, ϕ is the volume fraction of the colloidal particles and η_0 is the solvent viscosity. As the particle aspect ratio is increased, the intrinsic viscosity increases, and ϕ_m decreases, but the product of these two is usually in the range of $1.4 < [\eta]_s\phi_m < 3$.[18] The intrinsic viscosity of suspensions $[\eta]_s$ as formulated in eqn (3) is dimensionless, as it is defined in terms of the volume fraction. For an ideal dilute suspension of spherical particles, $[\eta]_s = 2.5$. If we examine the bulk viscosity data shown in Fig. 1, it is clear that the asymptotic plateau in the viscosity expected at low shear rates is not observed; the measured viscosity values at low deformation rates are significantly higher than anticipated for a protein of the size and shape of BSA, and this has led to the extensive discussion in the literature regarding formation of colloidal crystals by relatively small concentrations of globular proteins.[3–12] The concentration dependence observed in the high shear rate viscosity (η_∞) measurements (from the microfluidic capillary rheometer) follow the trend anticipated by the Krieger-Dougherty equation for a spherically shaped dispersed phase up to concentration of 100 mg ml^{-1} (see Fig. 6).

In protein and polymer solution rheology, the intrinsic viscosity is defined in terms of concentration, c (mg ml^{-1}), and is computed using $[\eta]_P = \lim_{c\to 0} -(\eta - \eta_0)/c\eta_0$. The intrinsic viscosity computed from the data in Fig. 6 is $[\eta]_P \approx 0.004$ ml mg^{-1} (4 ml g^{-1} or 0.04 dl g^{-1}) and this agrees well with the typical reported value of $[\eta]_P = 4.1 \pm 0.3$ ml g^{-1}.[55–59] Note that the intrinsic viscosity now has units of reciprocal concentration (ml g^{-1}). BSA is a globular protein with a molecular weight of 66 kDa and at neutral pH, fatty-acid-free BSA exists as a heart-shaped molecule, though conventionally the dispersed protein is modeled as an ellipsoid.[1,60] While anisotropy in shape affects both dynamics and self-assembly of colloidal particles,[18,61] the

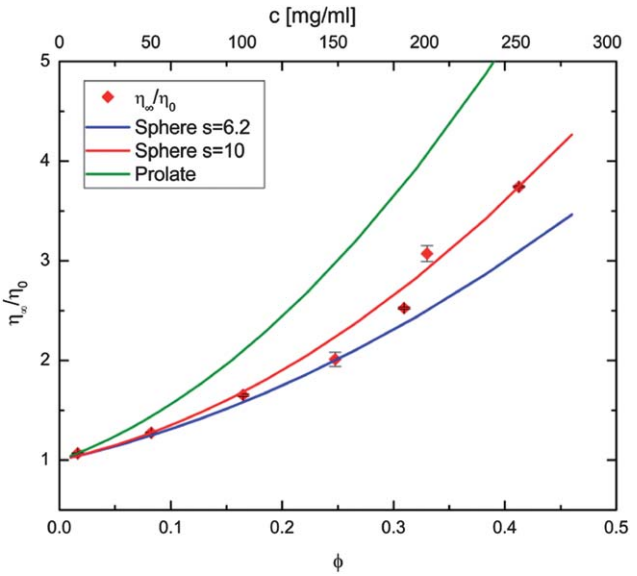

Fig. 6 Concentration dependence of the high shear rate viscosity of BSA (red symbols; measured in VROC) is fit by charged colloid theory, eqn (4) (red line). The bounds for uncharged prolate hard ellipsoids (green) and hard spheres (blue), eqn (3) (see text for details), are also shown.

reported aspect ratio of BSA is $L/d = 3.5$, and is thus rather small to anticipate formation of a liquid crystalline phase in bulk or at the interface. In any case, we see that the fit of eqn (3) for a prolate ellipsoid with $L/d = 3.5$ (green line in Fig. 6), estimated using Simha's formula,[57] over-predicts the viscosity.

If we use the diffusive time scales estimated earlier on the basis of solvent viscosity to be $t_D \approx 0.2$ μs even for an applied shear rate, $\dot{\gamma} = 10^4$ s^{-1}, the Peclet number (ratio of the diffusive to the flow contribution) is of the order of $Pe = \dot{\gamma}t_D \approx 0.002$. The Peclet number provides a measure of the perturbative effects due to flow compared to the restoring effect of Brownian motion;[17] low values of Pe implies that non-equilibrium effects often seen for colloidal suspensions with larger particles (>1 μm) are not present even in the microfluidic measurements. In other words, the concentration-dependent viscosity values $\eta_\infty(c)$ measured on VROC are in fact representative of the true zero shear viscosity for these protein solutions, and therefore we are justified in using these values in Fig. 6. We note, however, that for the protein concentrations studied here, the measurements in the microfluidic rheometer or VROC are shear-rate independent (or display Newtonian behavior), and therefore the extrapolation to lower shear rates will give the same viscosity value as measured, say, at a shear rate of 1000 s^{-1}. In the case of bulk viscosity measured by cone-and-plate (CP) or double-gap (DG) geometry, a similar extrapolation is not advisable and an inspection of Fig. 1b shows that the CP extrapolation will always give higher viscosity values than obtained by extrapolating DG data. For example, in studies on monoclonal antibody solutions,[34–36] where an apparent yield-like response is observed in bulk viscosity measurements, He *et al.*[34] choose to extrapolate the shear-thinning viscosity data (measured at high shear rates) in order to estimate zero-shear viscosity, without incorporating the yield-like response that is evident at low shear rates (see Fig. S1 in the ESI† of He *et al.*[34]). It is possible that this yield-like response also arises due to interfacial effects of the

kind we document in this work and this deviation could also be studied using the methodology described in this paper. The interfacial viscoelasticity—as well as the apparent bulk viscosity reported from torsional rheometers—will also be affected by the presence of surfactants and other surface-active groups, and in the particular case of monoclonal antibody solutions, the interfacial viscoelastic effects are commonly suppressed by addition of a non-ionic surfactant.[36]

The classic data by Tanford and Buzzell[55] that include measurements up to 40 mg ml^{-1} using capillary viscometers for BSA solutions are often discussed as a textbook example of the concentration dependence of viscosity expected for charged colloids.[17,18] The presence of surface charge increases the effective particle diameter, and concomitantly increases the viscosity observed at any volume fraction, ϕ.[17,18] The analysis by Russel[17,18] gives the viscosity in the form:

$$\frac{\eta(\phi)}{\eta_0} = 1 + 2.5\phi + \left(2.5 + \frac{3}{40}\left(\frac{d_{\text{eff}}}{a}\right)^5\right)\phi^2 + O(\phi^3)$$
$$= 1 + 2.5\phi + s\phi^2 + O(\phi^3) \quad (4)$$

The magnitude of s (*i.e.* the coefficient of the quadratic term) or the value of d_{eff} is dictated by the hydrodynamic contributions and interaction potential relevant to the specific dispersion being considered (higher charge implies larger d_{eff} and larger s, for example).[17,18] In general, the value of s depends upon specific interactions (and the model used), and for a system where only hard sphere repulsion applies ($d_{\text{eff}} = 2a$), Batchelor showed that $s = 6.2$. In Russel's formulation for the charged sphere case, the value of s is related to electrostatics, and usually $d_{\text{eff}} > 2a$. The concentration dependence of viscosity of BSA solution can be described by using eqn (4). The best fit value, $s = 10$, corresponds to an interaction potential of O(kT) as calculated theoretically for BSA solutions[62] using the classical Derjaguin–Landau–Verwey–Overbeek (DLVO) theory that describes the response of charge-stabilized colloidal particles in terms of electrostatic and dispersion interactions.[17,18]

It has been suggested[3–7] that the yield-like behavior observed in viscosity measurements on torsional rheometers arises from colloidal crystals formed by globular proteins that display long range interaction potentials with strengths up to $\sim 15kT$.[5] But these same researchers[3–7] also noticed the lack of any solid-like structure in scattering data and observed that neither the concentration of proteins nor addition of salts changes the magnitude of the measured viscoelastic response. A recent study recognized that the small angle neutron scattering (SANS) data indicate absence of crystal structure[11] and another recent study[10] went as far as measuring interfacial rheology for BSA solutions, but both studies cite the presence of colloidal crystals invoked by Ikeda and Nishinari.[5] Our interface-free bulk viscosity measurements demonstrate that the yield stress and high interaction potentials of $\sim 15kT$ result from systematic errors associated with fitting models to bulk rheology data that have a substantial interfacial contribution. Further, the value of s obtained from the fit, as described above, implies that the effective interparticle separation, $d_{\text{eff}} = 2.5a$. Since a hard sphere suspension can form a colloidal lattice within the bulk (or subphase) only when $\phi_{\text{eff}} = \phi(d_{\text{eff}}/2a)^3 > 0.55$, a colloidal lattice can be expected only at $\phi > 0.3$ or for $c > 200$ mg ml^{-1}. This implies that the bulk rheological properties of these proteins can be well described by existing models, provided the data are not corrupted by interfacial contributions. This comparison highlights the fact that the apparent viscosity measured by rotational rheometers needs to be evaluated most carefully whenever surface-active molecules or dispersants are involved.

More broadly speaking, we note that since the same thermodynamic interactions determine the absolute value of osmotic pressure and therefore of viscosity, diffusion coefficient and scattering intensity, among other properties,[17,63] the response from different measurements should be consistent with each other as long as the microstructure is the same. The concentration-dependent osmotic pressure, $\Pi(c)$ of dispersed colloidal particles or proteins[17,18] is given by $\Pi(c) = ckT[A_1 + A_2c + \ldots]$, where A_1 is related to size and A_2 is related to the interaction potential. For the pH and ionic content relevant to this study, the osmotic pressure of BSA solutions[12,64,65] corresponds to interaction potential of O(kT). Likewise, Minton and Edelhoch in 1982[63] were able to fit light scattering data of BSA solutions from Edsall *et al.*[66] with a model for charged colloidal suspension that describes the osmotic pressure, $\Pi(c)$, for BSA. Countless other studies on hydrodynamic properties of well-dispersed BSA that report intrinsic viscosity, sedimentation equilibrium and diffusion measurements[17,18,56–59,62,67–70] find interaction potentials of O(kT) and no evidence of any solid-like, long range structure in BSA solutions. Hence we conclude that the observed yield-like behavior observed in measurements on rotational rheometers arises in fact from the interfacial viscoelasticity of the adsorbed layer of proteins.

In colloidal dispersions, the yield stress presents a measure of interactions between the colloidal particles; these interactions are responsible for formation of a three-dimensional ordered macrolattice structure. Therefore, for colloidal dispersions, a simple first order estimate for yield stress can be made from the interaction potential[18,71] by using $\sigma_Y \approx \phi U/Kd_{\text{eff}}^3$, where K is an adjustable parameter (we use a typical value $K = 0.33$, see ref. 18 and 71 for additional discussion). If we select an interaction energy, $U \approx 15k_BT$ for the BSA solutions and use the value of bulk yield stress measured as 10^{-2} Pa (from our data and representative of values reported by Ikeda and Nishinari[5] and Regev *et al.*[10]), the effective interparticle separation, d_{eff} turns out to be $\sim$O(1 μm) which is two orders of magnitude larger than the protein size. On the other hand, if we use the actual measured interfacial yield stress $\sigma_{Ys} \approx 2 \times 10^{-4}$ Pa m, and an interaction energy $U \approx k_BT$, the effective interparticle distance estimated using the corresponding interfacial expression $\sigma_{Ys} \approx \phi_s U/Kd_{\text{eff}}^2$ turns out to be $d_{\text{eff}} \approx 6$ nm, which is close to the estimate obtained independently from the concentration dependence of viscosity. The high concentration of protein at the interface thus creates the apparent yield-like response. This yielding can be observed in both interfacial measurements and in the bulk rheology measurements whenever formation of a viscoelastic film can take place; for example when using a cone-and-plate geometry on a torsional rheometer.

3.5 Extracting interfacial viscosity contribution from bulk viscosity

In this section, we wish to show a simple but quantitative connection between the interfacial viscosity contribution, $\eta_s(\dot{\gamma})$

(measured by DWR) and the apparent bulk viscosity, $\eta(\dot{\gamma})$ of the protein solution measured by a torsional rheometer for the double-gap (DG) geometry (see ESI† for the corresponding cone-and-plate (CP) derivations). We assume that the thickness of the interfacial film is small compared to the characteristic dimension of the chosen geometry and that the measured torque, $M^{DG}(\dot{\gamma})$, from the rheometer is related to the shear stress contributed by the sub-phase fluid, $\tau_B = \eta_B\dot{\gamma}$ as well as to the interfacial contribution $\tau_s(\dot{\gamma}) = \eta_s(\dot{\gamma})\dot{\gamma}$ (units: Pa m), so that

$$M^{DG}(\dot{\gamma}) = 2[2\pi R(L-\delta)\tau_B + 2\pi R\delta(\tau_s/\delta)]R \quad (5)$$

The interfacial deformations are localized over a length scale, δ (see ESI†). The bulk viscosity of the BSA solutions at high shear-rates, η_∞ (measured in the VROC), approaches the true zero shear rate viscosity, as $\eta_\infty \approx \eta(\phi,\dot{\gamma} \to 0)$, implying that $\tau_B \approx \eta_\infty\dot{\gamma}$. Further, the interfacial contribution, shown in Fig. 3, can be modeled simply as a purely plastic or yielding event implying that the second term is given by $\tau_s = \tau_{sY} = G'_s\gamma_Y$, where the yield stress is obtained from oscillatory strain sweep measurements described earlier. The corresponding interfacial viscosity is then $\eta_s(\dot{\gamma}) \equiv \tau_{sY}/\dot{\gamma}$, and is strongly shear thinning. The total shear rate-dependent viscosity, $\eta(\dot{\gamma})$ (reported by rheometer), is then computed using the following formula

$$\eta(\dot{\gamma}) = \frac{M^{DG}(\dot{\gamma})}{4\pi R_i^2 L\dot{\gamma}} \approx \eta_B + l_G^{-1}\eta_s(\dot{\gamma}) \approx \eta_\infty + l_G^{-1}(\tau_{sY}/\dot{\gamma}) \quad (6)$$

Here the effective length scale, l_G, appearing in eqn (6) accounts for the different dimensionality of the interfacial and bulk viscosity contribution, and is derived from the torque expressions to be $l_G = L$ for the DG geometry (and $l_G = R/3$ for the CP; see ESI†). The close agreement between the measured value (symbols in Fig. 7) and computed values for each geometry (solid line) shows that this simple Bingham-like model of a Newtonian-like bulk stress and a plastic/yielding interfacial contribution provides a good *a priori* estimate of the actual viscometric data measured with a bulk rheometer. Finally we note that eqn (6) can also be written as $\eta(\dot{\gamma})/\eta_\infty \approx 1 + Bo_s^{DG}$ where $Bo_s^{DG} = (\tau_{sY}/\dot{\gamma})/\eta_\infty L$ is the relevant Boussinesq number for the DG geometry. The interfacial contribution is dominant only when $Bo_s > 10$, and this is indeed the case for these BSA solutions (see ESI† for additional discussion). Furthermore, at the highest shear rates, the Boussinesq number, Bo_s, reaches its lowest values, implying the interfacial contribution is weakest, and therefore the measurements from the DG geometry agree quite well with the interface-free microfluidic rheometer, as seen in Fig. 1a. Similarly, the reason for the discrepancy between the bulk data measured with the DG fixture and that measured with the CP fixture can be understood by a similar argument based on the Boussinesq number. The ratio of the wetted area to the perimeter in a cone-and-plate device is $l_s^{(CP)} \approx \pi R^2/2\pi R = R/2(\sim 10$ mm) compared to $l_s^{(DG)} \approx 2\pi RL/2\pi R = L(59.5$ mm) in the double gap fixture. The Boussinesq number is thus smaller in the DG fixture for any surface active complex fluid and the interfacial effects are correspondingly less important in the measured torque.

Alternatively, measurements of the apparent bulk viscosity, $\eta(\dot{\gamma})$ (measured with DG or CP), and the Newtonian viscosity, η_∞, measured in a microfluidic device (VROC) can be combined to estimate the rate-dependent interfacial viscosity contribution, by rearranging eqn (6) to give:

$$\eta_s(\dot{\gamma}) \approx l_G(\eta(\dot{\gamma}) - \eta_\infty) \quad (7)$$

Again the agreement between the estimates given by eqn (7) (dashed lines in Fig. 7) and data measured independently using DWR (symbols) shows that the simple additive model captures the general trends quite well. The quantitative discrepancy arises because of the larger coupling between the interfacial and sub-phase deformation in a torsional rheometer which is not reflected in the simple linear decomposition of eqn (6) and (7). A similar discrepancy arises if we use two separate bulk viscosity measurements and solve for the sub-phase viscosity and interfacial contribution using $\eta(\dot{\gamma}) \approx \eta_B + l_G^{-1}\eta_s(\dot{\gamma})$, where the geometry-dependent l_G is computed as described before. Thus, an accurate determination of the interfacial contribution requires the use of a device like DWR with a high Boussinesq number, though a combination of bulk measurements can provide a qualitative measure of the interfacial viscosity. Interestingly, the estimate of the interfacial contribution also explains why the apparent bulk viscosity measured in the cone-and-plate geometry is higher than that in the double gap geometry at all shear rates, as seen in Fig. 1a. The internal consistency between this simple Bingham-like additive model and these distinct measurement techniques is quite encouraging, and could prove useful for deconvolving interfacial effects in other complex biofluids.

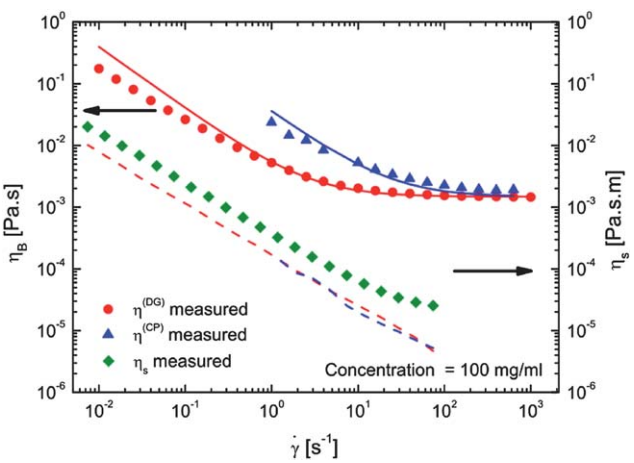

Fig. 7 Comparison of the measured shear-rate-dependent viscosity response (blue and red symbols) to the model behavior (solid lines) computed by using the effective Bingham model (eqn (6)) for a 100 mg ml^{-1} BSA solution as a function of shear rate. The model response has two contributions: the bulk contribution is calculated using the high shear rate viscosity measured using a microfluidic rheometer and the interfacial contribution is computed using the apparent yield stress obtained from oscillatory strain sweep measurements (solid lines). Also shown is a comparison of measured interfacial viscosity, η_s (DWR) (diamonds) with the estimates (dashed lines) extracted using eqn (7) (see text for details).

4. Conclusions

The kinetics of layer formation, the viscoelasticity and stability of the interface under applied deformation, and the intimate

coupling between interfacial and bulk viscosity behavior with shear rate tells us unambiguously that surfactant-free solutions of BSA (and possibly other globular proteins) form an interfacial film with rich viscoelastic behavior at the solution/gas interface. The DWR geometry attached to a torsional rheometer provides the resolution and sensitivity required to effectively isolate the contribution of the interfacial layer whereas the microfluidic capillary rheometer (VROC) eliminates any free surface effects to measure the correct value of steady shear viscosity (η_∞) at high shear rates. By contrast the measured or apparent viscosity obtained from rotational rheometers is superficially high due to the adsorbed interfacial protein film, and the relative bulk and interfacial contributions depend upon the specific test fixture selected. In this paper, we have investigated the interfacial and bulk properties independently, and shown that the osmotic pressure, diffusion coefficient, scattering and intrinsic viscosity measurements of BSA solutions can all be described self-consistently, and we do not need to invoke any special long-range interactions or colloidal microstructures. We provide a simple model that provides an understanding of the connection between the interfacial viscosity and bulk viscosity measurements.

It must be remarked here that serum albumins are important constituents of blood. Blood is a multi-component complex fluid that displays a highly non-Newtonian response to deformation amplitude and rate in bulk rheometry.[72] The apparent yield-like behavior provides blood with the necessary rheological properties required for the physiological function: it makes stopping blood flow easier, while providing low resistance (and low pumping cost) to deformations at high flow rates.[73] In fact, the contribution of serum albumins to overall blood rheology has been of long standing interest, and the early hemorheology literature[73–75] is dominated by the pioneering studies of Bingham, Blair, Copley, Ferry and Merrill. We refer specifically to a review,[73] where Merrill notes that the "*serum usually presents some form of experimental artifact in viscometry, attributable to a tendency toward rigid or semirigid surface films.*" As we have noted already, this seems to be neglected in many recent studies.[3–12] Further, Merrill[73] notes presciently that "*when the rotational viscometer is operated with a guard ring (which eliminates the interface) or when a capillary viscometer is operated such that flow rate is the imposed parameter and pressure gradient (measured by transducer in a gas free circuit) is the observed response, plasma and serum are Newtonian, down to zero strain rate and up to at least several inverse seconds of strain rate.*" Our results with the microfluidic rheometer show that the Newtonian regime in fact extends out to $\dot{\gamma} \geq 10^4$ s^{-1} for BSA solutions. While Merrill refers to studies in 1960s[73] that identified interfacial effects as the cause for apparent yield stress, the Newtonian response of serum was observed earlier by several researchers including Blair[75] and Tanford and Buzzell.[55] Apparently, more recent rheological studies on globular proteins[3–12] seem to be unaware of these historical studies, and their assertion that the apparent yield stress of globular proteins arises from an underlying colloidal crystal microstructure has started to propagate in the literature a somewhat erroneous idea that globular proteins have long-range interactions that are markedly stronger than electrostatic repulsions. Indeed, the interaction potential of O(kT) computed by using DLVO theory agrees very well with the interaction energy estimated by using the concentration dependence of the bulk viscosity as measured in the interface-free rheometer and independently computed from the interfacial yield stress measured using the double wall ring geometry.

We believe that this detailed study of bovine serum albumin solutions, in conjunction with reconsideration of early literature, will provide much needed clarification about the complex effects observed in the bulk rheology and interfacial viscoelasticity of globular proteins in particular, as well as other complex surface-active species in general. While the current study focused on surfactant-free protein solutions, the experimental protocol, and simple additive rheological model described herein can be adopted for the complex mixed interfaces expected for multicomponent biological and industrial fluids. While the interfacial viscosity of lung surfactants is known to play an important role in their functioning,[23] the physiological importance of interfacial viscosity and viscoelasticity of serum albumins, globular proteins, monoclonal antibodies and saliva remains to be elucidated. It is evident, however, that in designing synthetic biofluid replacements or pharmaceutical formulations containing surface active molecules, the formation, structure and rheological properties of interfaces must be taken into account, especially where the formation of a viscoelastic film at the liquid–air interface is known to occur.

Acknowledgements

VS acknowledges funding support from Akzo-Nobel. The authors thank Seong-gi Baek for stimulating our interest in this research, and TA Instruments for access to the DWR fixture.

References

1 T. Peters, *All about Albumin: Biochemistry, Genetics, and Medical Applications*, Academic Press, New York, 1996.
2 D. C. Carter and J. X. Ho, *Adv. Protein Chem.*, 1994, **45**, 153–203.
3 T. Matsumoto and H. Inoue, *Chem. Phys.*, 1993, **178**, 591–598.
4 H. Inoue and T. Matsumoto, *J. Rheol.*, 1994, **38**, 973–984.
5 S. Ikeda and K. Nishinari, *Biomacromolecules*, 2000, **1**, 757–763.
6 T. Matsumoto and H. Inoue, *Chem. Phys.*, 1996, **207**, 167–172.
7 H. Inoue and T. Matsumoto, *Colloids Surf., A*, 1996, **109**, 89–96.
8 S. Ikeda and K. Nishinari, *Int. J. Biol. Macromol.*, 2001, **28**, 315–320.
9 S. Ikeda and K. Nishinari, *Food Hydrocolloids*, 2001, **15**, 401–406.
10 O. Regev, S. Vandebril, E. Zussman and C. Clasen, *Polymer*, 2010, **51**, 2611–2620.
11 K. M. N. Oates, W. E. Krause, R. L. Jones and R. H. Colby, *J. R. Soc., Interface*, 2006, **3**, 167–174.
12 G. J. Brownsey, T. R. Noel, R. Parker and S. G. Ring, *Biophys. J.*, 2003, **85**, 3943–3950.
13 A. W. Adamson and A. P. Gast, *Physical Chemistry of Surfaces*, John Wiley & Sons, New York, 6th edn, 1997.
14 D. A. Edwards, H. Brenner and D. T. Wasan, *Interfacial Transport Processes and Rheology*, Butterworth-Heinemann, Boston, 1991.
15 *Interfacial Rheology*, ed. R. Miller and L. Liggieri, Brill, Leiden, 2009.
16 S. Vandebril, A. Franck, G. G. Fuller, P. Moldenaers and J. Vermant, *Rheol. Acta*, 2010, **49**, 131–144.
17 W. B. Russel, D. A. Saville and W. R. Schowalter, *Colloidal Dispersions*, Cambridge University Press, Cambridge, 1989.
18 R. G. Larson, *The Structure and Rheology of Complex Fluids*, Oxford University Press, New York, 1999.
19 T. van Vliet, A. H. Martin and M. A. Bos, *Curr. Opin. Colloid Interface Sci.*, 2002, **7**, 462–468.
20 E. Dickinson, *Colloids Surf., B*, 1999, **15**, 161–176.
21 B. S. Murray, *Curr. Opin. Colloid Interface Sci.*, 2002, **7**, 426–431.
22 B. S. Murray, *Curr. Opin. Colloid Interface Sci.*, 2007, **12**, 232–241.
23 J. A. Zasadzinski, J. Ding, H. E. Warriner, F. Bringezu and A. J. Waring, *Curr. Opin. Colloid Interface Sci.*, 2001, **6**, 506–513.
24 G. B. Proctor, S. Hamdan, G. H. Carpenter and P. Wilde, *Biochem. J.*, 2005, **389**, 111–116.
25 K. B. Song and S. Damodaran, *J. Agric. Food Chem.*, 1987, **35**, 236–241.

26 J. Wang, S. M. Buck and Z. Chen, *Analyst*, 2003, **128**, 773–778.
27 E. M. Freer, K. S. Yim, G. G. Fuller and C. J. Radke, *J. Phys. Chem. B*, 2004, **108**, 3835–3844.
28 E. M. Freer, K. S. Yim, G. G. Fuller and C. J. Radke, *Langmuir*, 2004, **20**, 10159–10167.
29 J. Kraegel, S. R. Derkatch and R. Miller, *Adv. Colloid Interface Sci.*, 2008, **144**, 38–53.
30 B. S. Murray, *Curr. Opin. Colloid Interface Sci.*, 2011, **16**, 27–25.
31 D. Langevin and F. Monroy, *Curr. Opin. Colloid Interface Sci.*, 2010, **15**, 283–293.
32 H. A. Waterman, C. Blom, H. J. Holterman, E. J. Sgravenmade and J. Mellema, *Arch. Oral Biol.*, 1988, **33**, 589–596.
33 M. S. Park, J. W. Chung, Y. K. Kim, S. C. Chung and H. S. Kho, *Oral Dis.*, 2007, **13**, 181–186.
34 F. He, G. W. Becker, J. R. Litowski, L. O. Narhi, D. N. Brems and V. I. Razinkov, *Anal. Biochem.*, 2010, **399**, 141–143.
35 J. Liu, M. D. H. Nguyen, J. D. Andya and S. J. Shire, *J. Pharm. Sci.*, 2005, **94**, 1928–1940.
36 T. W. Patapoff and O. Esue, *Pharm. Dev. Technol.*, 2009, **14**, 659–664.
37 C. Sanchez, D. Renard, P. Robert, C. Schmitt and J. Lefebvre, *Food Hydrocolloids*, 2002, **16**, 257–267.
38 P. Erni, P. Fischer, E. J. Windhab, V. Kusnezov, H. Stettin and J. Laüger, *Rev. Sci. Instrum.*, 2003, **74**, 4916–4924.
39 L. E. Scriven, *Chem. Eng. Sci.*, 1960, **12**, 98–108.
40 M. A. Bos and T. van Vliet, *Adv. Colloid Interface Sci.*, 2001, **91**, 437–471.
41 S. Reynaert, C. F. Brooks, P. Moldenaers, J. Vermant and G. G. Fuller, *J. Rheol.*, 2008, **52**, 261–285.
42 F. Ortega, H. Ritacco and R. G. Rubio, *Curr. Opin. Colloid Interface Sci.*, 2010, **15**, 237–245.
43 V. Prasad, S. A. Koehler and E. R. Weeks, *Phys. Rev. Lett.*, 2006, **97**, 176001.
44 D. T. Chen, E. R. Weeks, J. C. Crocker, M. F. Islam, R. Verma, J. Gruber, A. J. Levine, T. C. Lubensky and A. G. Yodh, *Phys. Rev. Lett.*, 2003, **90**, 108301.
45 A. J. Levine and T. C. Lubensky, *Phys. Rev. Lett.*, 2000, **85**, 1774–1777.
46 C. J. Pipe, T. S. Majmudar and G. H. McKinley, *Rheol. Acta*, 2008, **47**, 621–642.
47 P. Dhar, Y. Y. Cao, T. M. Fischer and J. A. Zasadzinski, *Phys. Rev. Lett.*, 2010, **104**, 4.
48 J. R. Lu, T. J. Su and R. K. Thomas, *J. Colloid Interface Sci.*, 1999, **213**, 426–437.
49 D. E. Graham and M. C. Phillips, *J. Colloid Interface Sci.*, 1979, **70**, 415–426.
50 L. G. C. Pereira, O. Theodoly, H. W. Blanch and C. J. Radke, *Langmuir*, 2003, **19**, 2349–2356.
51 D. E. Graham and M. C. Phillips, *J. Colloid Interface Sci.*, 1980, **76**, 227–239.
52 D. E. Graham and M. C. Phillips, *J. Colloid Interface Sci.*, 1980, **76**, 240–250.
53 T. F. Svitova, M. J. Wetherbee and C. J. Radke, *J. Colloid Interface Sci.*, 2003, **261**, 170–179.
54 A. K. Gaigalas, J. B. Hubbard, M. McCurley and S. Woo, *J. Phys. Chem.*, 1992, **96**, 2355–2359.
55 C. Tanford and J. G. Buzzell, *J. Phys. Chem.*, 1956, **60**, 225–231.
56 J. Lefebvre, *Rheol. Acta*, 1982, **21**, 620–625.
57 J. L. Richards, *J. Chem. Educ.*, 1993, **70**, 685–689.
58 D. E. McMillan, *Biopolymers*, 1974, **13**, 1367–1376.
59 S. E. Harding, *Prog. Biophys. Mol. Biol.*, 1997, **68**, 207–262.
60 M. L. Ferrer, R. Duchowicz, B. Carrasco, J. G. de la Torre and A. U. Acuna, *Biophys. J.*, 2001, **80**, 2422–2430.
61 V. Sharma, K. Park and M. Srinivasarao, *Mater. Sci. Eng., R*, 2009, **65**, 1–38.
62 E. Wajnryb and J. S. Dahler, *J. Colloid Interface Sci.*, 1999, **217**, 249–258.
63 A. P. Minton and H. Edelhoch, *Biopolymers*, 1982, **21**, 451–458.
64 V. L. Vilker, C. K. Colton and K. A. Smith, *J. Colloid Interface Sci.*, 1981, **79**, 548–566.
65 J. Z. Wu and J. M. Prausnitz, *Fluid Phase Equilib.*, 1999, **155**, 139–154.
66 J. T. Edsall, H. Edelhoch, R. Lontie and P. R. Morrison, *J. Am. Chem. Soc.*, 1950, **72**, 4641–4656.
67 G. I. Loeb and H. A. Scheraga, *J. Phys. Chem.*, 1956, **60**, 1633–1644.
68 P. G. Squire, P. Moser and C. T. Okonski, *Biochemistry*, 1968, **7**, 4261–4272.
69 A. Saluja and D. S. Kalonia, *J. Pharm. Sci.*, 2005, **94**, 1161–1168.
70 C. Tanford and J. Reynolds, *Nature's Robots*, Oxford University Press, Oxford, 2001.
71 D. Quemada and C. Berli, *Adv. Colloid Interface Sci.*, 2002, **98**, 51–85.
72 C. Picart, J. M. Piau and H. Galliard, *J. Rheol.*, 1998, **42**, 1–12.
73 E. W. Merrill, *Physiol. Rev.*, 1969, **49**, 863–888.
74 E. C. Bingham, *J. Gen. Physiol.*, 1945, **28**, 605–626.
75 G. W. S. Blair, *Nature*, 1959, **183**, 613–614.